Comparison of radar and in situ measurements of atmospheric turbulence

Florian Zink[1] and Robert A. Vincent
Department of Physics, University of Adelaide, Adelaide, South Australia, Australia

Edmund Murphy and Owen Cote
Battle Space Environment Division, Hanscom Air Force Base, Massachusetts, USA

Received 20 July 2003; revised 10 March 2004; accepted 22 March 2004; published 8 June 2004.

[1] We compare measurements of refractive index structure constant C_n^2 and energy dissipation rate ϵ by VHF radar with in situ observations by high-resolution thermosondes during a campaign near Adelaide, Australia, in August 1998. A total of 17 thermosonde soundings was performed within a distance of 120 km to the radar site. The variance between estimates of $\langle C_n^2 \rangle$ from backscattered radar power and in situ thermosonde observations is found to be comparable to the observed variance of the radar estimates due to temporal and spatial variations of the turbulent parameters (angle brackets denote average over the radar range resolution of 1 km). The high-resolution thermosonde observations allow us to test the applicability of the turbulent volume fraction model to the estimation of $\langle \epsilon \rangle$ from $\langle C_n^2 \rangle$. The data indicate that the turbulent volume fraction should not be modeled as the fraction of unstable layers with gradient Richardson number $R_i < 0.25$. *INDEX TERMS:* 3379 Meteorology and Atmospheric Dynamics: Turbulence; 3360 Meteorology and Atmospheric Dynamics: Remote sensing; 3694 Mineralogy and Petrology: Instruments and techniques; 6952 Radio Science: Radar atmospheric physics; *KEYWORDS:* turbulence, remote sensing

Citation: Zink, F., R. A. Vincent, E. Murphy, and O. Cote (2004), Comparison of radar and in situ measurements of atmospheric turbulence, *J. Geophys. Res.*, *109*, D11108, doi:10.1029/2003JD003991.

1. Introduction

[2] Atmospheric turbulence is usually characterized by the refractive index structure function constant C_n^2 or by the energy dissipation rate ϵ. Different techniques have been used in the past to measure these atmospheric turbulence parameters in situ. By recording velocity fluctuations along the flight path of an instrumented aircraft, the dissipation rate can be inferred from properties of the velocity spectrum or fluctuations in the vertical velocity field [*Chen*, 1974]. The evolution of smoke puffs [*Kellogg*, 1956] and vapor trails released from rockets [*Roper*, 1996] has also been studied using high-resolution photographs. The growth or diffusion rate of the trail provides information about the strength of local eddies. Another possibility is high-resolution balloon measurements of velocity and temperature [*Barat*, 1982; *Barat and Bertin*, 1984; *Luce et al.*, 1997] that allow calculation of spectra or direct measurement of the structure function constant.

[3] Radars offer an alternative means to monitor turbulence in the atmosphere, with a greatly improved time resolution compared with in situ methods. Radars are susceptible to refractive index irregularities on the scale of half the radar wavelength. Therefore radar echoes contain information about the density (returned power) and velocity distribution (spectral width) of refractive index irregularities of that scale within the radar sampling volume.

[4] The power and spectral width methods have been used in many radar studies to infer turbulence parameters in the lower and middle atmosphere [*Crane*, 1980; *Weinstock*, 1981; *Fukao et al.*, 1994; *Cohn*, 1995; *Hocking and Mu*, 1997; *Nastrom and Eaton*, 1997; *Gossard*, 1998; *Hooper and Thomas*, 1998; *Pepler et al.*, 1998; *Hermawan and Tsuda*, 1999; *Ghosh et al.*, 2003]. Because of the lack of colocated in situ observations, however, the validity of the radar measurements can often be justified only by the right order of magnitude of the derived turbulence parameters or by agreement with similar observations. While a few direct comparisons of VHF radar echoes with direct balloon estimates exist [*Eaton et al.*, 1988; *Luce et al.*, 1997], further case studies are needed.

[5] In this paper we compare measurements of refractive index structure function constant C_n^2 and energy dissipation rate ϵ by VHF radar and thermosondes during a campaign near Adelaide, Australia, in August 1998. Because of the coarse height resolution of the radar (1 km) the spectral width of the radar returns is dominated by spatial fluctuations due to gravity waves. We therefore limit our analysis

[1] Now at deCode Genetics Inc., Reykjavik, Iceland.

0148-0227/04/2003JD003991

to estimates of turbulence parameters derived from backscattered power measurements.

2. Methods

2.1. Determination of $\langle C_n^2 \rangle$ by Radar

[6] Radars are susceptible to refractive index irregularities on the scale of half the radar wavelength λ. For VHF radar in the troposphere and lower stratosphere this scale lies within the inertial subrange of turbulence. The backscattered power can therefore be used to infer the magnitude of the refractive index structure function constant $\langle C_n^2 \rangle$, if the inhomogeneities in the radar sampling volume are due to inertial range turbulence. Here angle brackets denote average over the radar sampling volume. Using the backscattering cross section for isotropic, homogeneous turbulence [*Tatarskii*, 1961]

$$\sigma^{\text{scat}} = 0.00655\pi^{4/3} C_n^2 \lambda^{-1/3}, \tag{1}$$

one obtains

$$\langle C_n^2 \rangle = c \frac{P_r}{r^2}, \tag{2}$$

where P_r is the radar power backscattered from range r and c is a constant. While it is possible to determine c by careful calibration of radar and antenna systems, we simply use the proportionality between the signal power at the receiver output to $\langle C_n^2 \rangle r^2$ and estimate the proportionality constant by comparing values of $\langle C_n^2 \rangle$ obtained from hourly averaged radar spectra and thermosonde for all sonde flights during the campaign. While this procedure disregards any possible bias between the two methods, it does not affect our ability to estimate the variance between radar and thermosonde measurements.

2.2. Relationship Between ϵ and C_n^2

[7] For homogeneous, isoptropic, and stationary turbulence the refractive index structure function constant C_n^2 can be expressed as [*Ottersten*, 1969; *Weinstock*, 1981]

$$C_n^2 = a^2 \epsilon^{2/3} \frac{R_f}{1 - R_f} \frac{M^2}{N^2}, \tag{3}$$

where $a^2 = 2.8$ [*VanZandt et al.*, 1978], N is the buoyancy frequency, and R_f is the flux Richardson number. The potential refractive index gradient M is defined as

$$M = -77.6 \times 10^{-8} \frac{p}{T} \frac{\partial \ln \Theta}{\partial z} \left[\underbrace{1 + \frac{15500q}{T} \left(1 - \frac{1}{2} \frac{\frac{\partial \ln q}{\partial z}}{\frac{\partial \ln \Theta}{\partial z}} \right)}_{\chi} \right], \tag{4}$$

where p is the atmospheric pressure (Pa), T is the temperature (K), Θ is the potential temperature (K), and q is the specific humidity (g/kg). The term in brackets, χ, accounts for contributions due to humidity. As equation (3) shows, turbulence manifests itself in refractive index inhomogeneities only for $M \neq 0$. That is, turbulent layers are only observable by radar if the potential temperature or the specific humidity differs with height.

[8] Because of the nonlinearities in equation (3) a model has to be invoked to estimate $\langle \epsilon \rangle$ from measurements of $\langle C_n^2 \rangle$. A frequently applied model assumes that a volume fraction F of the radar sampling volume is filled with turbulent layers of (equal) energy dissipation rate ϵ and refractive index structure function constant C_n^2 and that the contributions from the remaining sampling volume to $\langle \epsilon \rangle$ and $\langle C_n^2 \rangle$ are negligible. Assuming further that the ratio of N^2 and M^2 does not vary much throughout the sampling volume, one obtains

$$\langle \epsilon \rangle = \left(\frac{1}{a^2} \frac{1 - R_f}{R_f} \frac{\langle C_n^2 \rangle N^2}{F^{1/3} M^2} \right)^{3/2}. \tag{5}$$

The turbulent volume fraction F itself is usually estimated either from modeling studies or from high-resolution observations as the fraction of unstable layers with gradient Richardson number $R_i < 0.25$ [*VanZandt et al.*, 1978].

3. Instrumentation and Data Processing

3.1. Buckland Park VHF Radar

[9] The Buckland Park VHF radar operates at a frequency of 54.1 MHz with 32 kW peak power. The antenna system consists of two orthogonal coaxial-collinear (CoCo) antenna arrays of around 8000 m^2. The beam steering capability of the system is achieved by inserting phase delay cables between the transmitter and the antenna rows. The CoCo arrays are used for both transmission and reception in Doppler mode.

[10] During the campaign the radar was used in a five-beam Doppler beam steering configuration with parameters as given in Table 1. A zenith angle of 14.5° was chosen for off-zenith beams to ensure that the backscattered power is due to isotropic turbulence and is not contaminated by Fresnel scatter or reflection so that equation (1) can be applied [*Hocking et al.*, 1990].

[11] The radar data are analyzed by taking all L time series for a given beam pointing angle and range bin within the time window of an hour and dividing each of them into M segments of equal length (M is determined by the required frequency resolution and was set to 3 in our analysis; L is around 12). After detrending with a low-order polynomial to remove ground clutter [*May and Strauch*, 1998], the periodograms for each of the ML segments are computed and averaged using the statistical averaging method (SAM) as described by *Merritt* [1995]. In short, for each frequency bin the largest power estimate is removed iteratively until the standard deviation σ of the remaining power estimates is less than or equal to their mean μ. The SAM assumes that the power estimates for atmospheric signals plus noise are χ^2 distributed with 2 degrees of freedom (one each for the in-phase and in-quadrature components), such that $\mu = \sigma$ and that clutter distributions are from the high-power tail of the distribution. The mean μ of the remaining power estimates is then used as the power estimate of the considered frequency bin. Finally, the mean noise level is estimated using the method of *Hildebrand and Sekhon* [1974], and the location of the signal peak in the averaged periodogram is determined.

[12] Furthermore, we performed consistency checks in height and time and with the opposite beam direction. The

Table 1. Radar Configuration During the Turbulence Campaign

Beam	14.5° N, S, E, W	Vertical Beam
Pulse repetition frequency, s^{-1}	4,096	4,096
Coherent integrations	256	512
Dwell time, s	56.25	50
Sampling ranges, m	1,200–19,200	1,200–19,200
Range resolution, m[a]	1,000	1,000

[a]500 m oversampled.

incoherent averaging increases the height range of usable radar returns for several kilometers, while the statistical clutter removal gets rid of airplane echoes in the radar signals, an acute problem with the Buckland Park radar due to its location close to the flight path of a busy airport. Knowing the location of the signal peak from the hourly averaged spectra, we then estimated noise and signal power for the contributing 1-min spectra for a narrow frequency range centered around this location. While the hourly averaged spectra provide us with reliable estimates of noise and signal power, the data from the nonaveraged 1-min spectra yield information about the temporal variation of these estimates.

3.2. Thermosondes

[13] The thermosonde is attached to a standard GPS radiosonde package and measures fine-scale temperature differences across a fixed horizontal distance of 1 m. This signal is then filtered and averaged to compute a running temperature structure function, where a time constant of 3.75 s is used. The structure function is sampled every 1.2 s by a spare channel of the radiosonde and is relayed to the ground station together with the temperature, pressure, humidity, and wind data from the radiosonde. To minimize perturbations of the measurements by the wake of the balloon, the instrumentation gondola is attached to the balloon using a line of 100 m length.

[14] The running average of the differential temperature measurements ΔT at a distance of 1 m directly yields the temperature structure function constant $C_T^2 = \overline{\Delta T^2}$. In the absence of humidity this can be converted to C_n^2 by

$$C_n^2 = \left(77.6 \times 10^{-8} \frac{p}{T^2}\right)^2 C_T^2. \quad (6)$$

[15] The radar and thermosonde data are obtained with different altitude resolutions. The radar has a resolution of 1 km, while the thermosonde has an average height resolution of about 20 m. To allow a comparison of the two data sets, the thermosonde data were convolved with the radar resolution. We used a triangular window of the same width as the radar pulse as convolution kernel for profiles of ϵ and C_n^2 to obtain the corresponding averages (denoted by angle brackets) over the radar sampling volume.

[16] While we treat the in situ thermosonde measurements as our reference, these data are also subject to error and can deviate from the true atmospheric parameters. *Jumper et al.* [1999] investigated possible error sources in thermosonde measurements, including pendular motion, strong thermal gradients, and regions of non-Kolmogorov turbulence. They estimated that the integrated circuit used to compute the output signal may exaggerate the turbulence by 20–30%.

[17] Three thermosondes were launched daily after sunset for 6 consecutive days at Gawler (34°37′S, 138°44′E). Figure 1 shows the thermosonde trajectories relative to the radar site for the 6 campaign days. Crosses along the trajectories mark 5-km height intervals up to 20 km.

4. Results and Discussion

4.1. Comparison of the Average Refractive Index Structure Function Constant $\langle C_n^2 \rangle$

[18] Profiles of $\langle C_{n,\mathrm{radar}}^2 \rangle$ for hourly averaged radar spectra were computed as described in section 2.1 and were averaged over the four available beam directions. Thermosonde measurements of C_T^2 were first converted to C_n^2 using equation (6) and then were convolved with the radar resolution to obtain $\langle C_{n,\mathrm{sonde}}^2 \rangle$. To account for the fact that the radar is susceptible to gradients in specific humidity while the thermosonde is not, we correct the thermosonde profiles for humidity effects by multiplication with $\langle \chi \rangle^2$ (equation (4)).

[19] Figure 2 compares profiles of $\langle C_n^2 \rangle$ as obtained with the two different methods for the three soundings on 24 August 1998. The thin solid and dashed lines correspond to thermosonde measurements with and without humidity correction applied, respectively. The thick solid lines indicate values deduced from the hourly averaged radar spectra.

[20] The humidity correction increases the values of $\langle C_{n,\mathrm{sonde}}^2 \rangle$ between 1 and 2 orders of magnitude up to a height of 10 km. It is noteworthy that the humidity-corrected profiles of $\langle C_{n,\mathrm{sonde}}^2 \rangle$ agree well with the profiles of $\langle C_{n,\mathrm{radar}}^2 \rangle$ over the whole height range (except for the deviation at 5 km for the launch at 1155 UTC), even in the troposphere where the humidity correction is large. As the thermosonde is only susceptible to inhomogeneities in temperature, it will miss turbulent layers for which the potential temperature gradient vanishes (even after the humidity correction is applied), while the radar can still see those layers because of the presence of specific humidity gradients. The deviation of the profiles at 5 km for the launch at 1155 UTC might be explained by real atmospheric differences between the radar and thermosonde locations, as the radar profile is very similar to the profile for the launch at 1008 UTC at this height, where it was in good agreement with the sonde profile of that time.

[21] In order to get some insight into the variability of the measurements, Figure 2 also includes the interquartile

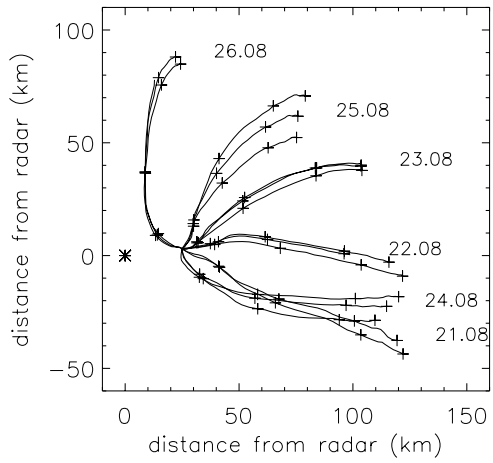

Figure 1. Map of the thermosonde trajectories relative to the radar site (designated by a star at the origin). Crosses along the trajectories mark 5-km height intervals.

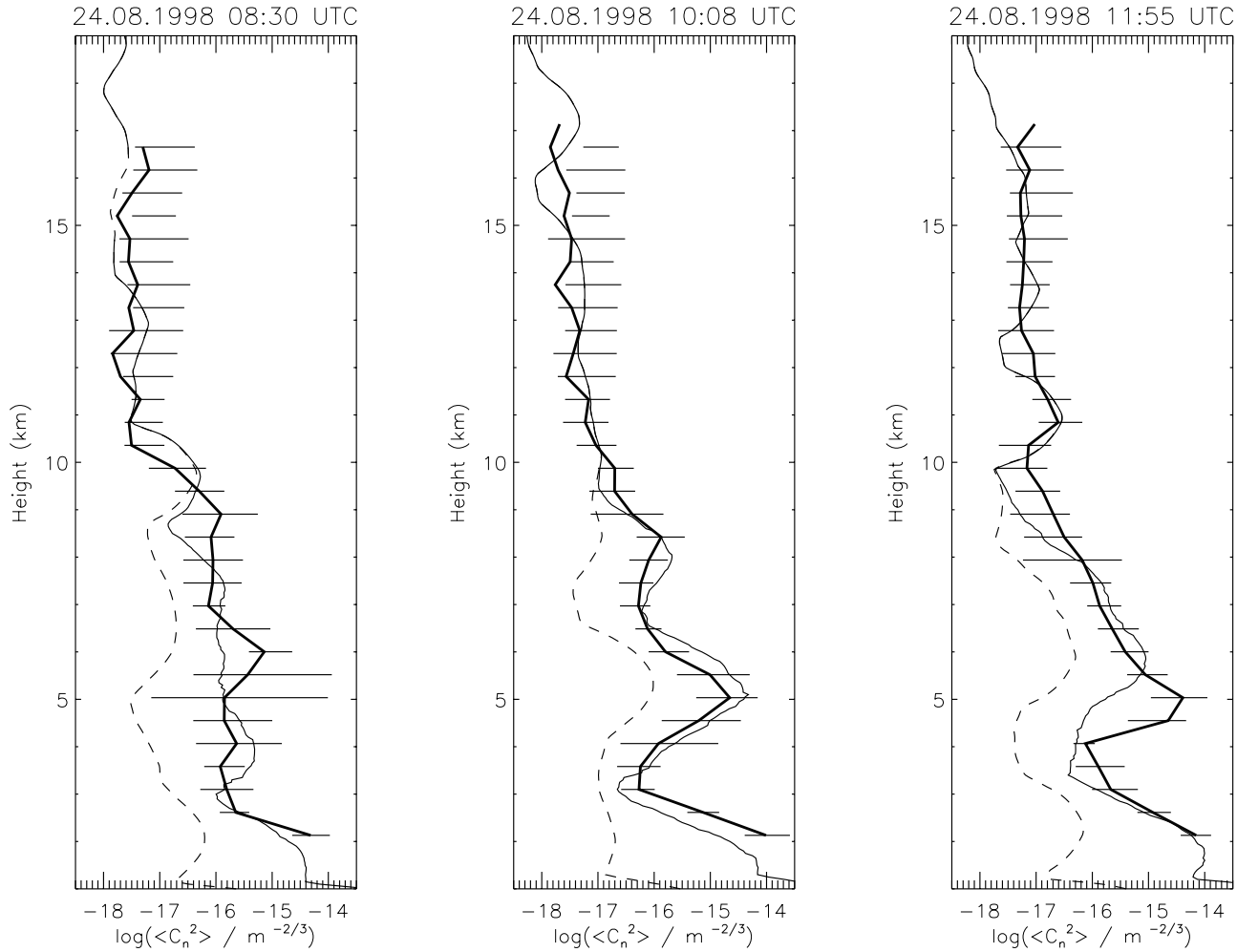

Figure 2. Profiles of average refractive index structure function constant $\langle C_n^2 \rangle$ as measured by radar and thermosonde for the three soundings of 24 August. The thin solid and dashed lines correspond to thermosonde measurements with and without humidity correction, respectively. The thick solid lines indicate profiles deduced from hourly averaged radar spectra, while the horizontal bars illustrate the interquartile range of estimates obtained from the 1-min radar spectra within 1 hour around the sonde flight.

range (25th to 75th percentile) of $\langle C_{n,\mathrm{radar}}^2 \rangle$ as obtained from the 1-min spectra within 1 hour around the sounding (horizontal bars). For lower heights the variance in $\langle C_{n,\mathrm{radar}}^2 \rangle$ as obtained from different spectra is indicative of temporal fluctuations in $\langle C_n^2 \rangle$, while at larger heights, uncertainties in the determination of the signal power P_r become important. The plots also show that the minimum detectable $\langle C_n^2 \rangle$ for the hourly averaged spectra is significantly reduced compared with the 1-min spectra. Values of $\langle C_n^2 \rangle$ as deduced from the 1-min spectra reach their background level above a height of about 12 km, while the hourly averaged spectra yield reliable results up to a height of 17 km.

[22] The variations in $\langle C_n^2 \rangle$ as seen by the radar are a combination of both spatial and temporal variations as the atmosphere is advected through the radar sampling volume. Their magnitude therefore gives some indication about the expected deviations between the profiles of $\langle C_{n,\mathrm{radar}}^2 \rangle$ and $\langle C_{n,\mathrm{sonde}}^2 \rangle$ at their respective locations. This is in agreement with the displayed profiles, for which the deviations between the two profiles are of similar magnitude as the variation observed with the radar.

[23] Figure 3 (top) shows a histogram of $\log\langle C_{n,\mathrm{radar}}^2 \rangle / \langle C_{n,\mathrm{sonde}}^2 \rangle$ for the 17 soundings of the campaign. A Gaussian fit to the data (dashed line) shows that this ratio is approximately lognormal distributed with a standard deviation $\sigma = 0.32$; that is, measurements of $\langle C_n^2 \rangle$ by radar and thermosonde agree within a factor of 2.1 (1 standard deviation). These deviations are of similar size as the variations observed by radar and hence lies within expectations. A scatterplot of $\langle C_{n,\mathrm{radar}}^2 \rangle$ versus $\langle C_{n,\mathrm{sonde}}^2 \rangle$ for the same data is presented in Figure 3 (bottom). The largest scatter can be observed for large values of $\langle C_n^2 \rangle$ corresponding to tropospheric heights, where additional uncertainties are introduced through application of the humidity correction.

4.2. Comparison of the Average Energy Dissipation Rate $\langle \epsilon \rangle$

[24] The refractive index structure function constant C_n^2 and the energy dissipation rate ϵ are related through equa-

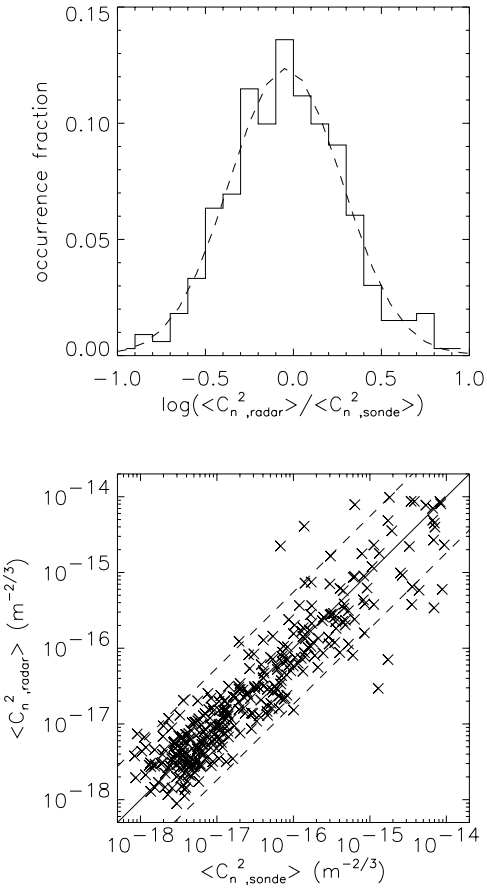

Figure 3. (top) Comparison of $\langle C_n^2 \rangle$ measurements obtained by radar and thermosonde during the 6 days of the campaign. The ratio of $\langle C_{n,\mathrm{radar}}^2 \rangle$ to $\langle C_{n,\mathrm{sonde}}^2 \rangle$ is approximately lognormal distributed with a standard deviation of $\sigma = 0.32$. (bottom) Same data as a scatterplot. The dashed lines correspond to the 95% confidence interval.

tion (3), in which the buoyancy frequency N and the potential refractive index gradient M are considered atmospheric background parameters. It is not clear a priori, however, at what spatial resolution these parameters should be used in application of the theory.

[25] *Bertin et al.* [1997] performed high-resolution balloon soundings of the stratosphere and directly measured turbulent velocity and temperature fluctuations within seven turbulent layers. Their observations show that the potential temperature gradient is strongly eroded by turbulent mixing within fully developed turbulent layers. This results in a refractive index structure constant C_n^2 that is strongly reduced within the layer and exhibits maxima on its boundaries, while the turbulent velocity structure constant $C_V^2 = 2\epsilon^{2/3}$ is approximately constant throughout the layer.

[26] For high-resolution measurements of C_n^2, which can resolve single turbulent layers, this implies that the above "background" parameters have to be applied at a spatial resolution comparable to the layer thickness in order to reconcile the observations of C_n^2 and C_V^2. For layers with $N^2/M^2 \approx 0$, however, ϵ will be badly defined, and large uncertainties result. Measurements with a lower resolution, like radar, on the other hand, will only be able to resolve layers with large C_n^2, where the potential temperature gradient has not been eroded; that is, only initial stage turbulence or the boundaries of fully developed turbulent layers will be observable. For these measurements, the uneroded, i.e., low resolution, profiles of these background parameters will be applicable.

[27] The authors also observe that the gradient Richardson number R_i varies significantly throughout the layer, with small values where the temperature gradient and C_n^2 are small and large values at the layer boundaries, where C_n^2 exhibits maxima. The flux Richardson number R_f, on the other hand, stayed within a range of about 0.15...0.3 throughout the observed turbulent layers. The authors therefore conclude that high-resolution measurements of the energy dissipation rate ϵ using equation (3) with $R_f = 0.25$ should be accurate within a factor of 2 to 3.

[28] Following *Bertin et al.* [1997], we compute the energy dissipation rate for the thermosonde from high-resolution profiles of potential temperature using equation (3) with $R_f = 0.25$ and $\chi = 1$ as

$$\epsilon = \left[\frac{3}{2.8}\frac{N^2 C_T^2}{\left(\frac{\mathrm{d}\Theta}{\mathrm{d}z}\right)^2}\right]^{3/2} = \left[\frac{3}{2.8}\frac{g C_T^2}{\Theta \frac{\mathrm{d}\Theta}{\mathrm{d}z}}\right]^{3/2}, \tag{7}$$

where g is the acceleration due to gravity. In order to avoid large uncertainties in ϵ due to small gradients in potential temperature Θ, we restrict ourselves to heights above 10 km. The profiles of ϵ are, subsequently, convolved with the radar resolution to yield $\langle \epsilon_{\mathrm{sonde}} \rangle$.

[29] The computation of $\langle \epsilon_{\mathrm{radar}} \rangle$ is complicated by the fact that because of the nonlinear relationship of ϵ and C_n^2 in equation (3) the volume fraction of turbulent layers in the radar sampling volume appears in equation (5). The volume fraction model assumes that the layers dominating $\langle \epsilon_{\mathrm{radar}} \rangle$ also dominate $\langle C_{n,\mathrm{radar}}^2 \rangle$ and, furthermore, that these layers are identifiable by $R_i < 0.25$. Both of these assumptions are somewhat in contrast with the in situ observations of *Bertin et al.* [1997]. First, as the gradient of potential temperature can vary considerably within a radar range, layers with very different values of C_n^2 can have similar values of ϵ. Second, while the condition $R_i < 0.25$ might identify turbulent layers, these layers are not necessarily the layers with the largest values of C_n^2 within the radar range.

[30] The availability of 17 high-resolution thermosonde soundings enables us to test the applicability of the volume fraction model on a larger data set. From the thermosonde data we compute the theoretical value of F as

$$F = \left[\frac{3}{2.8}\frac{g\langle C_T^2 \rangle}{\langle \Theta \rangle \frac{\mathrm{d}\langle \Theta \rangle}{\mathrm{d}z}}\right]^3 / \langle \epsilon_{\mathrm{sonde}} \rangle^2, \tag{8}$$

where angle brackets denote average over the radar sampling volume as usual. Note that we use the background profile of potential temperature at the radar resolution, as discussed above. The value F_{obs} was computed as the observed fraction of instable layers with gradient Richardson number $R_i < 0.25$, as calculated from high-resolution soundings. Figure 4 (top) shows histograms for $\log(F_{\mathrm{obs}})$ and $\log(F)$ with (geometric) means of $\overline{F_{\mathrm{obs}}} = 0.15$ and $\overline{F} = 0.23$, respectively. Note that the extremely small values of F

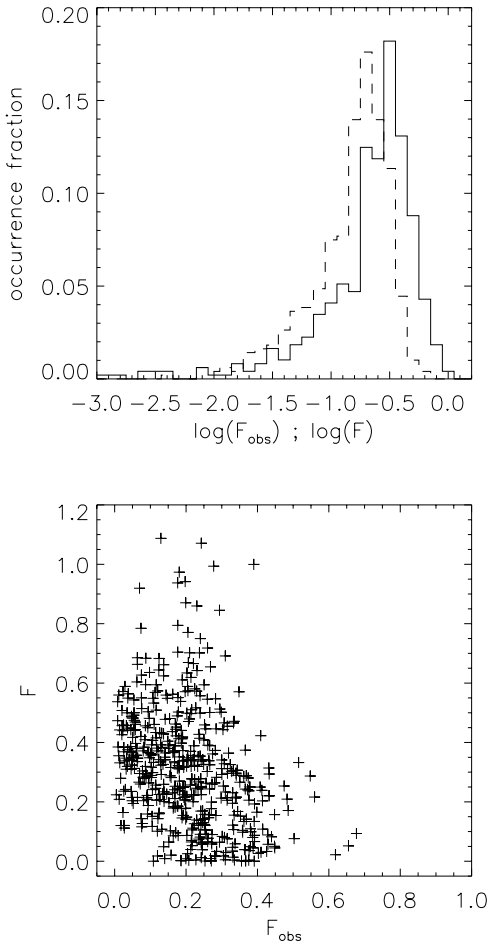

Figure 4. (top) Histograms of the distributions of theoretical F (solid line) and observed turbulent volume fraction F_{obs} (dashed line) for the 17 thermosonde soundings at heights above 10 km. (bottom) Same data as a scatterplot.

are due to large values of $\langle\epsilon_{sonde}\rangle$ in equation (8). The corresponding large values of ϵ are likely due to small gradients of potential temperature and hence have large uncertainties, which translate into large uncertainties in F. While the distributions of F and F_{obs} do not appear too dissimilar, the scatterplot in Figure 4 (bottom) reveals that F_{obs} and F are negatively correlated; that is, large values of F tend to correspond to small values of F_{obs} and vice versa.

[31] This behavior can be understood at least qualitatively. Assume a height interval with very little turbulent activity, i.e., $F_{obs} \approx 0$. For a constant gradient of potential temperature this translates to profiles of ϵ and C_n^2 that are relatively uniform with height. Therefore the whole height interval will contribute to $\langle C_n^2\rangle$ and $\langle\epsilon\rangle$ and F will be close to 1. For a very turbulent height interval with F_{obs} large, on the other hand, the observations of *Bertin et al.* [1997] show that C_n^2 can be strongly reduced within the turbulent layer. It is therefore mainly the boundaries of the turbulent layer that contribute to $\langle C_n^2\rangle$, corresponding to a small value of F.

[32] Modeling F as the fraction of layers with $R_i < 0.25$ would therefore increase the variance between values of $\langle\epsilon_{radar}\rangle$ and $\langle\epsilon_{sonde}\rangle$ compared with the application of a constant value F^o. In our comparison of $\langle\epsilon_{radar}\rangle$ and $\langle\epsilon_{sonde}\rangle$ we computed $\langle\epsilon_{radar}\rangle$ using a constant value of $F^o = \overline{F} = 0.23$. Note that the meaning of F^o is that of a fitting parameter to achieve agreement between the two methods. Figure 5 (top) shows a histogram of $\log(\langle\epsilon_{radar}\rangle/\langle\epsilon_{sonde}\rangle)$ for the 17 soundings during the campaign. As mentioned above, we restricted ourselves to height ranges above 10 km in order to avoid large uncertainties in $\langle\epsilon_{sonde}\rangle$ due to layers with small potential temperature gradients. A Gaussian fit to the data reveals a standard deviation of $\sigma = 0.45$; that is, values of $\langle\epsilon_{radar}\rangle$ and $\langle\epsilon_{sonde}\rangle$ deviate by a factor of 2.9 (1 standard deviation). If only measurements of $\langle C_n^2\rangle$ are available, F^o cannot be determined, and application of the volume fraction model can lead to a large bias in estimates of $\log\langle\epsilon\rangle$. Uncertainties in values of $\langle\epsilon\rangle$ as determined from measurements of $\langle C_n^2\rangle$ can therefore be considerably larger than indicated here.

[33] While the choice of a value $F^o \neq \overline{F}$ will bias profiles of $\log\langle\epsilon\rangle$, the variation of the profiles with height will not change. Figure 5 (bottom) shows a scatterplot of our data. The 95% confidence interval indicates that the average energy dissipation levels between radar ranges have to

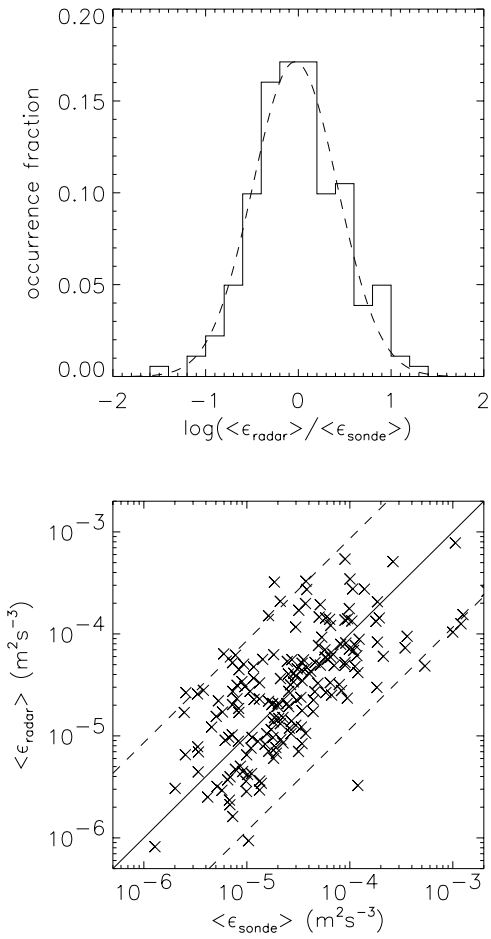

Figure 5. (top) Comparison of $\langle\epsilon\rangle$ measurements obtained by radar and thermosonde above 10 km during the 6 days of the campaign. The ratio of $\langle\epsilon_{radar}\rangle$ to $\langle\epsilon_{sonde}\rangle$ is approximately lognormal distributed with a standard deviation of $\sigma = 0.45$. (bottom) Same data as a scatterplot. The dashed lines correspond to the 95% confidence interval.

differ about an order of magnitude in order to be reliably distinguished by the radar method.

5. Summary

[34] We measured the average refractive index structure function constant $\langle C_n^2 \rangle$ and energy dissipation rate $\langle \epsilon \rangle$ using VHF radar and thermosondes during a 6-day campaign in August 1998. The high-resolution data from 17 thermosonde soundings were convolved with the radar range resolution of 1 km to allow comparison of the two data sets. The radar was calibrated by comparison of all concurrent $\langle C_n^2 \rangle$ measurements by radar and thermosonde available for the campaign.

[35] Height profiles of $\langle C_n^2 \rangle$ using hourly averages of backscattered radar power agree well with humidity-corrected measurements by the thermosonde throughout the observed height range of 2–18 km. The measurements of the two methods are within a factor of 2.1 of each other (1 standard deviation) for values of $\langle C_n^2 \rangle$ ranging from 10^{-18} to 10^{-14} $m^{-2/3}$.

[36] In order to convert radar measurements of the refractive index structure function constant $\langle C_n^2 \rangle$ into estimates of energy dissipation rate $\langle \epsilon \rangle$, information about the turbulent volume fraction F within the radar sampling volume is needed. While F is usually modeled as the fraction of layers with a gradient Richardson number $R_i < 0.25$, our simulation using the high-resolution thermosonde data shows that this procedure leads to an increased variance of $\langle \epsilon \rangle$ compared with a model where F is a constant. Using a constant F determined from comparison with the thermosonde data, estimates of energy dissipation rate $\langle \epsilon \rangle$ by radar and thermosonde are found to be within a factor of 2.9 of each other (1 standard deviation) for measurements above 10 km.

[37] The measurements are found to agree well, considering (1) the horizontal separations of up to 120 km between radar and thermosonde, (2) the fact that the thermosonde makes instantaneous measurements while the radar averages over a time window of 1 hour, and (3) the temporal variations of radar estimates within the averaging window.

[38] **Acknowledgments.** The radar studies were supported by Australian Research Council grant A1003317. We thank two anonymous reviewers for comments that led to significant improvement of the manuscript.

References

Barat, J. (1982), Some characteristics of clear-air turbulence in the middle stratosphere, *J. Atmos. Sci.*, *39*, 2553–2564.

Barat, J., and F. Bertin (1984), On the contamination of stratospheric turbulence measurements by wind shear, *J. Atmos. Sci.*, *41*, 819–827.

Bertin, F., J. Barat, and R. Wilson (1997), Energy dissipation rates, eddy diffusivity, and the Prandtl number: An in situ experimental approach and its consequences on radar estimates of turbulent parameters, *Radio Sci.*, *32*, 791–804.

Chen, W. Y. (1974), Energy dissipation rates of free atmospheric turbulence, *J. Atmos. Sci.*, *31*, 2222–2225.

Cohn, S. A. (1995), Radar measurements of eddy dissipation rate in the troposphere: A comparison of techniques, *J. Atmos. Oceanic Technol.*, *12*, 85–95.

Crane, R. K. (1980), A review of radar observations of turbulence in the lower stratosphere, *Radio Sci.*, *15*, 177–193.

Eaton, F. D., W. A. Peterson, J. R. Hines, K. R. Peterman, R. E. Good, R. R. Beland, and J. H. Brown (1988), Comparisons of VHF radar, optical, and temperature fluctuation measurements of C_n^2, r_0 and θ_0, *Theor. Appl. Climatol.*, *39*, 17–29.

Fukao, S., M. D. Yamanaka, N. Ao, W. K. Hocking, T. Sato, M. Yamamoto, T. Nakamura, T. Tsuda, and S. Kato (1994), Seasonal variability of vertical eddy diffusivity in the middle atmosphere: 1. Three-year observations by the middle and upper atmosphere radar, *J. Geophys. Res.*, *99*, 18,973–18,987.

Ghosh, A. K., A. R. Jain, and V. Sivakumar (2003), Simultaneous MST radar and radiosonde measurements at Gadanki (13.5°N, 79.2°E): 2. Determination of various atmospheric turbulence parameters, *Radio Sci.*, *38*(1), 1014, doi:10.1029/2000RS002528.

Gossard, E. E. (1998), Measurement of clear-air gradients and turbulence properties with radar wind profilers, *J. Atmos. Oceanic Technol.*, *15*, 321–342.

Hermawan, E., and T. Tsuda (1999), Estimation of turbulence energy dissipation rate and vertical eddy diffusivity with the MU radar RASS, *J. Atmos. Sol. Terr. Phys.*, *61*, 1123–1130.

Hildebrand, P. H., and R. S. Sekhon (1974), Objective determination of the noise level in Doppler spectra, *J. Appl. Meteorol.*, *13*, 808–811.

Hocking, W. K., S. Fukao, T. Tsuda, and S. Kato (1990), Aspect sensitivity of stratospheric VHF radio scatterers, particularly above 15 km altitude, *Radio Sci.*, *25*, 613–627.

Hocking, W. K., and P. K. L. Mu (1997), Upper and middle tropospheric kinetic energy dissipation rates from measurements of $\overline{C_n^2}$: Review of theories, in situ investigations, and experimental studies using the Buckland Park atmospheric radar in Australia, *J. Atmos. Sol. Terr. Phys.*, *59*, 1779–1803.

Hooper, D. A., and L. Thomas (1998), Complementary criteria for identifying regions of intense atmospheric turbulence using lower VHF radar, *J. Atmos. Sol. Terr. Phys.*, *60*, 49–61.

Jumper, G. Y., R. R. Beland, and P. Tracy (1999), Investigating sources of error in balloon-borne optical turbulence measurements, *Tech. Rep. AIAA 99-3618*, Am. Inst. of Aeronaut. and Astronaut., Reston, Va.

Kellogg, W. W. (1956), Diffusion of smoke in the stratosphere, *J. Meteorol.*, *13*, 241–250.

Luce, H., F. Dalaudier, M. Crochet, and S. Sidi (1997), An improved interpretation of VHF oblique radar echoes by a direct balloon C_n^2 estimation using a horizontal pair of sensors, *Radio Sci.*, *32*, 1261–1268.

May, P. T., and R. G. Strauch (1998), Reducing the effect of ground clutter on wind profiler velocity measurements, *J. Atmos. Oceanic Technol.*, *15*, 579–586.

Merritt, D. A. (1995), A statistical averaging method for wind profiler Doppler spectra, *J. Atmos. Oceanic Technol.*, *12*, 985–995.

Nastrom, G. D., and F. D. Eaton (1997), Turbulence eddy dissipation rates from radar observations at 5–20 km at White Sands Missile Range, New Mexico, *J. Geophys. Res.*, *102*, 19,495–19,505.

Ottersten, H. (1969), Atmospheric structure and radar backscattering in clear air, *Radio Sci.*, *4*, 1179–1193.

Pepler, S. J., G. Vaughan, and D. A. Hooper (1998), Detection of turbulence around jet streams using a VHF radar, *Q. J. R. Meteorol. Soc.*, *124*, 447–462.

Roper, R. G. (1996), Rocket vapor trail releases revisited: Turbulence and the scale of gravity waves: Implications for the imaging Doppler interferometry/incoherent scatter radar controversy, *J. Geophys. Res.*, *101*, 7013–7017.

Tatarskii, V. I. (1961), *Wave Propagation in a Turbulent Medium*, McGraw-Hill, New York.

VanZandt, T. E., J. L. Green, K. S. Gage, and W. L. Clark (1978), Vertical profiles of refractivity turbulence structure constant: Comparisons of observations by the Sunset Radar with a new theoretical model, *Radio Sci.*, *13*, 819–829.

Weinstock, J. (1981), Using radar to estimate dissipation rates in thin layers of turbulence, *Radio Sci.*, *16*, 1401–1406.

O. Cote and E. Murphy, Battle Space Environment Division, Air Force Laboratory, 29 Randolph Road, Hanscom AFB, MA 07131-3010, USA. (ocote@plh.af.mil; edmund.murphy@hanscom.af.mil)

R. A. Vincent, Department of Physics, University of Adelaide, Gate 13 Kintore Avenue, Adelaide, SA 5005, Australia. (robert.vincent@adelaide.edu.au)

F. Zink, deCode Genetics Inc., Sturlugata 8, 101 Reykjavik, Iceland. (fzink@physics.adelaide.edu.au)